Control of an articulated wheeled mobile robot in pipes

doi: 10.1080/01691864.2019.1666737

To appear in *Advanced Robotics*
Vol. 00, No. 00, January 2019, 1–20

Full Paper

Control of an articulated wheeled mobile robot in pipes

Hidemasa Sawabe[a]* , Mizuki Nakazima[a], Motoyasu Tanaka[a], Kazuo Tanaka[a] and Fumitoshi Matsuno[b]

[a] *The University of Electro-Communications, 1-5-1 Chofugaoka, Chofu, Tokyo, Japan*;
[b] *Kyoto University, Kyotodaigaku-katsura, Nishikyo-ku, Kyoto, Japan*

(*v1.0 released January 2019*)

We propose a control method in which an articulated wheeled mobile robot moves inside straight, curved and branched pipes. This control method allows the articulated wheeled mobile robot to inspect a larger area. The articulated wheeled mobile robot comprises pitch and yaw joints is and propelled by active wheels attached to the robot. Via the proposed control method, the robot takes on two different shapes; one prevents the robot from slipping inside straight pipes and the other allows movement in a pipe that curves in any direction. The robot is controlled by a simplified model for the robot's joint angles. The joint angles of the robot are obtained by fitting to a continuous curve along the pipe path. In addition, the angular velocity of the robot's active wheels is determined by a simplified model. The effectiveness of the proposed the control method was demonstrated with a physical implementation of the robot, and the robot was able to move inside straight, curved and branched pipes.

Keywords: Articulated mobile robot, Pipe, Snake robot

1. Introduction

Many pipes are installed in buildings and industrial facilities. It is difficult to enter and inspect the interiors of these pipes. Robots that inspect the inside pipe have therefore been developed [1]. The robots in [1] have different types of moving mechanisms; i.e., wheeled, tracked, legged, inchworm, snake and screw mechanisms. Inside pipes, the robots are prevented from slipping so they can move in various directions.

Thus, the robots dedicated to the pipe inspection have highly mobile performance inside pipes. The robots in [2–7] press against the pipe wall with active wheels and move inside the pipes by rotating these wheels. In [3], the wheel is a crawler type, and in [4] the wheel units are connected to each other. In [5–7], the robot wheels are linked with the joints, and the robot bends each joint alternately to form a zigzag shape that prevents it from slipping; additionally, these robots can rotate around the direction of movement.

These robots, which are specialized in terms of moving inside a pipe, have difficulty moving outside a pipe. Articulated mobile robots can move in narrow spaces and on uneven terrains, and these robots are used for pipe inspection, as described in [8–14]. The locomotion produced by a *sinusoidal wave drive* [8] allows a snake-like robot without wheels to move inside vertical pipes, pipes with different diameters, and curved pipes. A snake-like robot moves inside a straight pipe with *concertina movement* [15]. In this movement, parts of a snake body repeatedly lock and loosen from the head to tail, and the robot moves forward. In [9], the concertina movement was investigated in terms of self-locking when the snake robot climbs in a narrow space. The

*Corresponding author. Email: hidemasa.sawabe@rc.mce.uec.ac.jp

KAEROT-snake IV [10] climbs inside a vertical pipe using an inchworm motion. In [11, 12], to move on and inside pipes, a robot forms its shape into a helix to match its size to the pipe diameter, and then it laterally rolls its body to move forward. This method allows the robot to move through on a pipe with a branch [16], inside a T-joint pipe [11], and inside pipes with different diameters [13]. In addition, the robot moves over a pipe with a flange, on uneven terrain, and over ladders [14, 17].

A pipe-inspection robot needs to move along various routes before reaching the pipe entrance and after exiting from the pipe. Thus, its performance requirement includes moving both over complex terrain and inside pipes. Active-wheeled robots, which can move over the complex terrain, have been proposed for pipe inspection [18, 19].

We have developed an articulated wheeled mobile robot that can be used for both site inspection during disasters and equipment inspection in daily use [20, 21]. The robot can enter a narrow space or horizontal pipe, move over obstacles, climb steep stairs, and turn a valve by a wireless remote control. Industrial facilities have various terrains and inspection targets. If the robot can move inside pipes, the area that the robot can reach enlarges. Pipes contain obstacles, such as pipe joints, and have various shapes, for example, circular and rectangular. The articulated wheeled mobile robot, which can move over complex terrain [20, 21], is expected to be useful for pipe inspection. However, this robot does not have a mechanism specialized for pipe inspection, for example, a mechanism that pushes against the pipe wall to avoid slippage between the robot and pipe wall. Thus, it is difficult for this type of robot to move inside pipes, especially vertical pipes and curved pipes, by the existing control method. In addition, the helical rolling motion of [11, 12] cannot be applied for this articulated wheeled mobile robot.

The traditional method of controlling an articulated mobile robot is *shift control*, in which the motion of the head unit shifts from the head to tail of the robot. The operator easily operates the robot with shift control by providing only the head motion. In a method of *approximating a continuous curve* [22], the target of the body shape is represented as a continuous curve (*backbone curve* in [23]) and the joint angle of the robot is calculated by approximately fitting the body of the robot to the continuous curve. Shift control is then performed by shifting the area representing the body of the robot on the target curve. However, if the robot moves inside pipes using shift control, it is difficult to prevent the robot from slipping inside a vertical pipe.

In this paper, we aim at enlarging the inspection area of an articulated wheeled mobile robot and propose a control method by which the robot can move inside straight, curved and branched pipes. The robot uses two different shapes, one for straight pipe and the other for curved pipes. The shape for a straight pipe prevents the robot from slipping inside a straight pipe, and the shape for a curved pipe allows movement inside pipes that curve in any direction. The robot moves inside pipes with both straight and curved sections by switching between the two shapes with proper timing and active wheel turning. The effectiveness of the proposed the control method was demonstrated with experiments. In [24, 25], switching between scaffold-based locomotion and concertina locomotion was accomplished on a two-dimensional surface using the decentralized control scheme. Adopting this method, the behavior of the robot is affected by the influence of the surrounding environment without changing the parameters. As a result, the robot moves in an environment where both terrain with several pegs and a narrow aisle exists. Using this method, the robot moves in various environments using the same parameters, and there are thus few opportunities to set parameters. In contrast, because the parameters are determined by trial and error, the initial setting is performed several time and it is difficult to specify the moving speed and route of the robot's head accurately. Meanwhile, because the method proposed in this paper expresses the target route using a continuous curve, it can be linked to the movement using the three-dimensional steering method in [20]. This means that the articulated mobile robot with the structure of [20] can move through a pipe as well as on conventional terrain. Although [24, 25] and our research have different approaches, the goal of a single robot moving in various environments is the same. The advantage of our method over [24, 25] is that the operator can freely design the moving direction and velocity of the head of

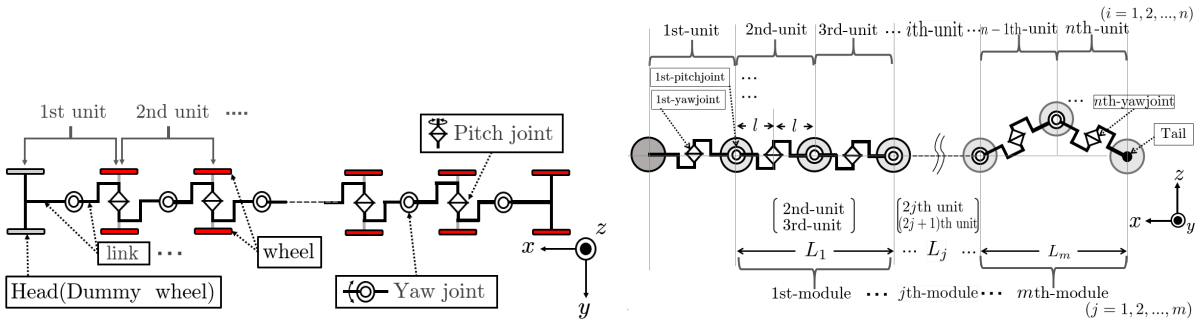

(a) Model of articulated wheeled mobile robot.

(b) Composition of joint, unit, and module in the robot.

Figure 1. An articulated wheeled mobile robot.

the robot using a continuous curve. Sensors and a camera are generally mounted on the head of a robot. The method is therefore effective in the explicit design of the leading movement path when performing remote control and inspection using sensors.

2. Model and environment

Figure 1 shows the model of an articulated wheeled mobile robot [20, 26]. The links of the robot are connected in series by alternating pitch and yaw joints. Two wheels are attached to the robot at the pitch joints coaxially and at the tail units. One or both of the two side wheels of each unit are active simultaneously. The wheels of the head unit are not driven. The robot is propelled by active wheels and the robot's shape is changed by rotating the joints. The configuration of the robot's joints and wheels is similar to that in the ACM-R4 series [27, 28]. Robots adopting this configuration have accomplished the avoidance of movable obstacles by switching the allocation of grounded wheels [26]. In addition, it can climb a high step and stairs because the rotational range of the pitch joint of the robot is wide [20].

Each unit i includes the $2i-1$-th link, i-th yaw joint, $2i$-th link, and i-th pitch joint. Note that the tail (n-th) unit does not have a pitch joint. Each pair of units, except the head (1st) unit, forms a module; for example, the j-th module includes the $2j$-th unit and the $2j+1$-th unit. Let l be the length of a link, L_j be the length of a module, n be the number of units ($i = 1, 2, ..., n$), and m be the number of modules ($j = 1, 2, ..., m$). The values of n and m satisfy $n = 2m + 1$. The angle of the i-th yaw joint and pitch joint are defined as ϕ_i and ψ_i, respectively.

The environment is the inside of the pipe composed of straight and curved segments, as shown in Figure 2, where two straight segments are connected by a curved segment. The radii of the pipe entrance and exit are equal. Constant values were assumed for the length of straight segments, the curvature of the curved segment, and the radius of all segments. The initial position of the robot is inside straight pipe because it can enter the pipe by the existing control method [20].

3. In-pipe locomotion

The robot moves inside a pipe that is vertical to the ground. In addition, the robot needs to move in any direction along the pipe. The robot types PIKo [18] and OT-4 [19], which have the active joints and the propulsion mechanism (active wheel or crawler), press the propulsion mechanism against the inside pipe wall by bending at the joints and move inside a vertical pipe by driving with the propulsion mechanism. When a robot inspects the interior of a pipe that includes straight, curved, and branching segments, it needs not only to move inside a vertical

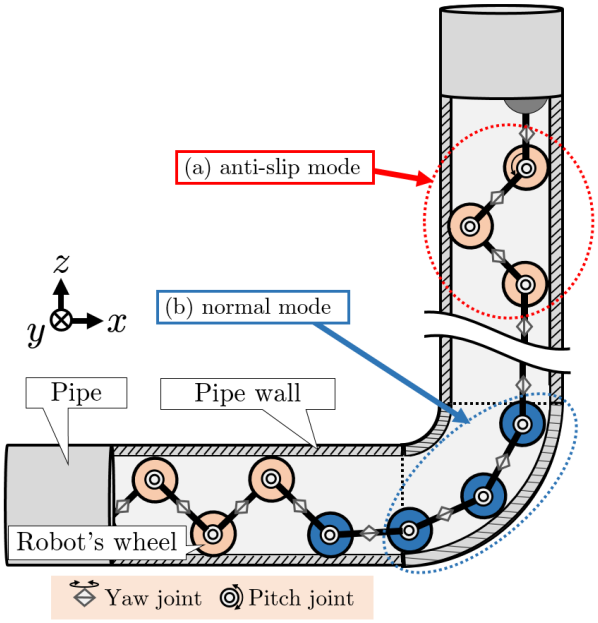

Figure 2. Proposed in-pipe locomotion for an articulated wheeled mobile robot.

pipe but also to turn in any direction.

We propose the in-pipe locomotion shown in Figure 2 for an articulated wheeled mobile robot. This locomotion allows the robot to move inside pipes that curve in any direction while avoiding slippage between the robot wheels and the pipe wall. The robot uses two shape modes, one for straight segments, as shown in Figure 2(a), and the other for curved segments, as shown in Figure 2(b). The shape mode for a straight pipe is used to avoid slippage between the robot wheel and pipe wall. We call this the *anti-slip mode*. In this mode, the yaw-joint angle is zero, and the body shape is made to zigzag by rotating the pitch joints. The robot presses its wheels against the inside pipe wall to prevent slipping. In contrast, the shape mode for a curved pipe, as shown in Figure 2(b), is called the *normal mode*. The reason for using the normal mode is that the yaw-joint angle of a module cannot be changed when the module is in anti-slip mode. Thus, when a robot module passes through a curved pipe, we change its mode from anti-slip to normal, as shown in Figure 3(a). As a result, the yaw joint can rotate without limitation. A module that is in normal mode can bend in any direction inside a curved pipe by changing the angle of the pitch and yaw joints.

In the proposed locomotion, the shape is appropriately switched between the two modes. First, all modules of the robot in a straight pipe are made anti-slip mode. As the robot moves forward, part of it enters a curved segment. Then, the modules that are in the curved segment are switched from anti-slip mode to normal mode, as shown in Figure 3(a). As the robot continues to move forward, some modules exit from the curved segment and enter the next straight segment. Then, the modules that have entered the straight segment are switched from normal mode to anti-slip mode to prevent the robot from slipping, as shown in Figure 3(b).

Each module of the robot should be switched the mode at an appropriate timing. In this paper, the motion that changes a module from anti-slip mode to normal mode is called *extension*, and the motion that changes a module from normal mode to anti-slip mode is called *contraction*. Because the assumed environment has only one curved segment, extension is always performed before a module enters the curved segment and contraction is always performed after a module exits from the curved segment. We assume that extension and contraction are not performed at the same time. If they overlap each other, the extension is performed after contraction is complete.

The PIKo [18] and OT-4 [19] types avoid slipping in a vertical pipe by adopting a wave shape

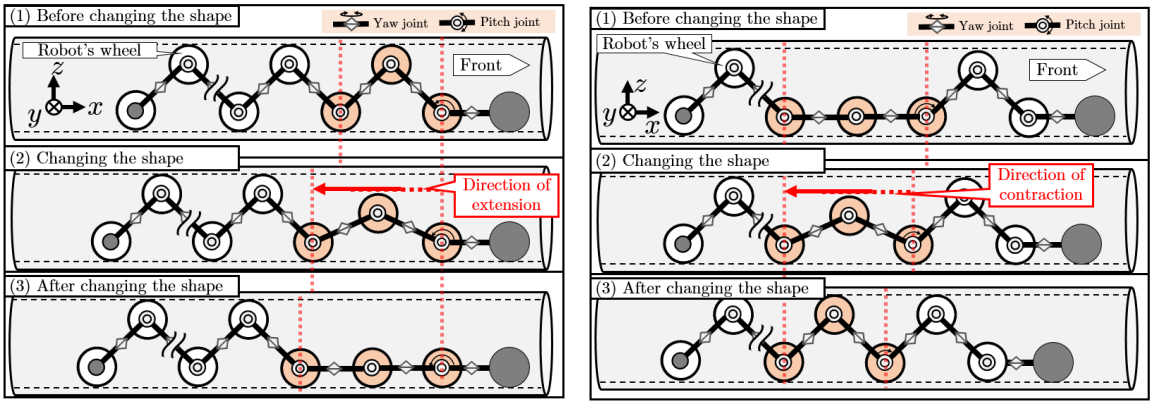

(a) Extension motion to assume normal mode (b) Contraction motion to assume anti-slip mode

Figure 3. The robot uses two shape modes inside a pipe.

as the overall posture. In contrast, the locomotion proposed in this paper uses as few as two units to avoid in-pipe slipping. If two units do not generate enough force to avoid slipping, the force for avoiding slippage can be increased by increasing the number of units that are in anti-slip mode. In addition, the robot can generate a large propulsion force because all active wheels of modules that are in anti-slip mode are in contact with the pipe wall. Moreover, the physical relationship between the number of modules that are in anti-slip mode and the force for avoiding slippage can be analyzed. For a robot using the helix rolling motion [11, 12], the head camera laterally rotates and its view needs to be adjusted for operation. In contrast, the proposed method avoids the need to adjust the direction of the camera view.

4. Simplified model for shift control

The robot in [22, 29] locomotes by shifting its head position on the continuous curve (*backbone curve* in [23]) from head to tail. However, if the method of [22, 29] is directly used, the robot cannot locomote in a vertical pipe because the robot cannot maintain the zigzag posture of the module in an anti-slip mode. Figure 4 shows an example of motion when using the method of [22, 29]. We therefore shift motion not by link but by module to keep the zigzag posture. When a module is switching between modes or it is in anti-slip mode, the motion of the module is shifted module by module. When a module is in normal mode, the motion is shifted link by link. As a result, the shift control is performed without changing the zigzag posture of modules that are in anti-slip mode.

In this paper, we use a *simplified model*, which is the model simply representing the shape of the robot for the shift control, as shown in Figure 5. For a module that is in normal mode, the positions of the joint of the simplified model is located at the positions of the yaw and pitch joints. For a module that is in anti-slip mode, the center pitch joint and the two yaw joints are ignored in the simplified model. In the simplified model, the number of the joints and the j-th module length (defined as L_j) change when the module mode changes.

5. Control

Figure 6 shows a flowchart for the robot control procedure. First, a target continuous curve that follows the pipe path is designed. Second, the operator inputs $s_{\mathrm{h,add}}$ and ω_{add}, where $s_{\mathrm{h,add}}$ is the displacement of the robot's head on the continuous curve and ω_{add} is the additional rotational

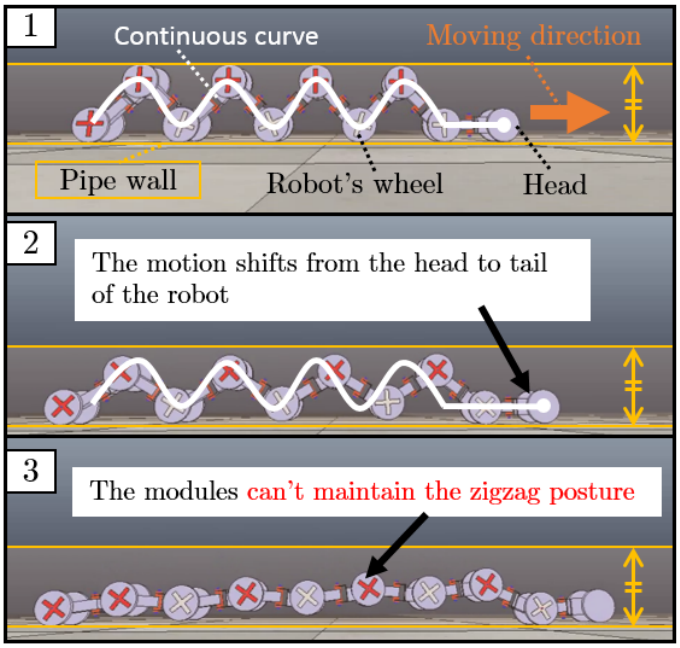

Figure 4. Robot motion during link-based shift control (the physical simulator V-REP [30] is used).

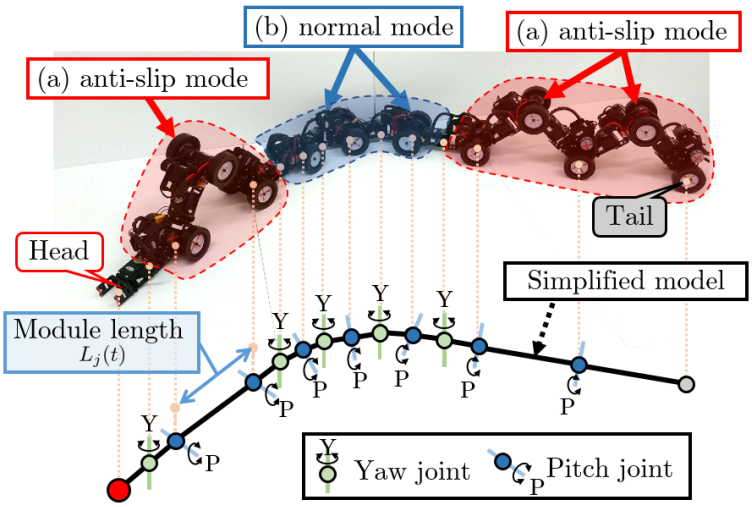

Figure 5. Simplified control model.

velocity of the active wheel. Third, the joint angles of the simplified model are calculated to fit the robot's shape to the target continuous curve by using a method of approximating a continuous curve [22, 29]. Fourth, the joint angles of the realistic model are calculated by converting from the simplified model to the realistic model. Finally, the rotational velocity of the active wheels is determined.

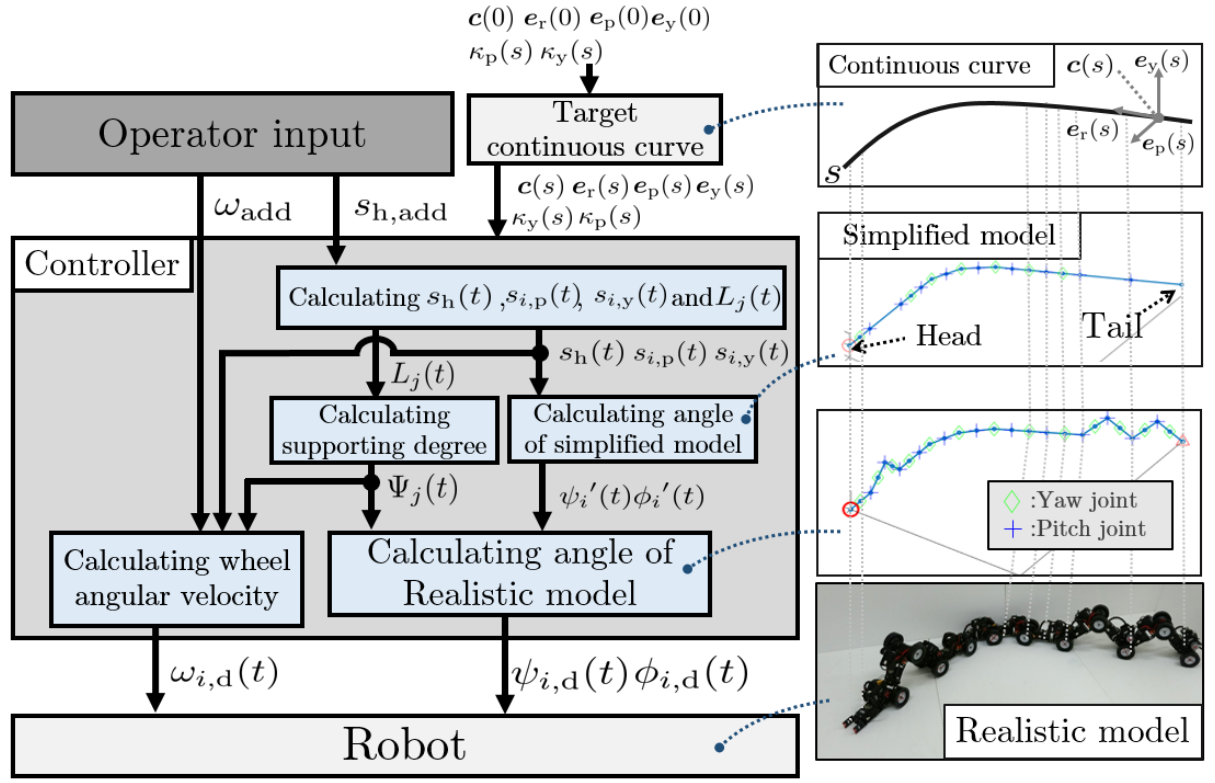

Figure 6. Flowchart for robot control.

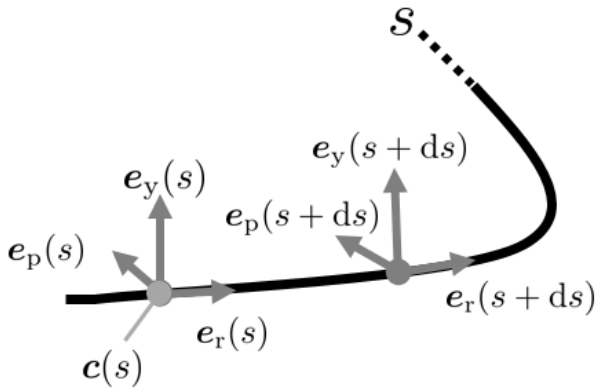

Figure 7. Target continuous curve.

5.1 *Continuous curve*

Figure 7 shows a target continuous curve, which is determined using the representation in [22, 29] as

$$\begin{cases} \dfrac{\mathrm{d}\boldsymbol{c}(s)}{\mathrm{d}s} = \boldsymbol{e}_{\mathrm{r}}(s) \\ \dfrac{\mathrm{d}\boldsymbol{e}_{\mathrm{r}}(s)}{\mathrm{d}s} = \kappa_{\mathrm{y}}(s)\boldsymbol{e}_{\mathrm{p}}(s) - \kappa_{\mathrm{p}}(s)\boldsymbol{e}_{\mathrm{y}}(s), \\ \dfrac{\mathrm{d}\boldsymbol{e}_{\mathrm{p}}(s)}{\mathrm{d}s} = -\kappa_{\mathrm{y}}(s)\boldsymbol{e}_{\mathrm{r}}(s) \\ \dfrac{\mathrm{d}\boldsymbol{e}_{\mathrm{y}}(s)}{\mathrm{d}s} = \kappa_{\mathrm{p}}(s)\boldsymbol{e}_{\mathrm{r}}(s) \end{cases} \tag{1}$$

where s is the length variable along the curve; ds is the infinitesimal difference of s; and $\boldsymbol{c}(s)$ is the positional vector that represents the coordinate of the continuous curve, which is $\boldsymbol{c}(s) = [x(s), y(s), z(s)]^{\mathrm{T}}$. The Cartesian coordinate system ($\boldsymbol{e}_{\mathrm{r}}(s)$,$\boldsymbol{e}_{\mathrm{p}}(s)$,$\boldsymbol{e}_{\mathrm{y}}(s)$) represents the posture of the robot's model, where $\kappa_{\mathrm{p}}(s)$ and $\kappa_{\mathrm{y}}(s)$ are the curvature around the pitch and yaw, respectively. On the continuous curve, the head position is $s_{\mathrm{h}}(t)$, the position of the i-th yaw joint is $s = s_{i,\mathrm{y}}$, and the position of the i-th pitch joint is $s = s_{i,\mathrm{p}}$. Note that $s_{n,\mathrm{p}}$ represents the tail position because the tail unit does not have a pitch joint.

5.2 *Positions of the head, tail and joints*

The timing of switching the modes is determined from $s_{\mathrm{h,add}}$ and the difference of the curvature on the continuous curve. The module during extension or contraction moves in a direction away from the curved pipe section. In Figure 3(a), which shows the extension of the first module, the position of the first pitch joint is fixed, and the following modules move back. In Figure 3(b), which shows the contraction of second module, the position of the fifth pitch joint is fixed, and the modules from the head to the fifth yaw joint move back. The aforementioned motions are performed by changing $L_j(t)$ and adjusting s_{h}. $L_j(t)$ is designed as

$$L_j(t) = L_j(t_s) + k(t - t_s), \tag{2}$$

where the time when the mode starts to change is $t = t_s$, k is a constant value, and $k > 0$ during extension and $k < 0$ during contraction. When the jth module is in normal mode, $L_j = 4l$. When the jth module is in anti-slip mode, $L_j = L_{\mathrm{min}}$. When the jth module is extending or contracting, $L_{\mathrm{min}} < L_j < 4l$. L_{min} is the module length that prevents the robot from slipping inside the pipe, and it is determined from the dimensions of the robot and pipe.

The adjustment of s_{h} is determined from $s_{\mathrm{h,add}}$ and the mode change. Thus, $s_{i,\mathrm{p}}(t)$ and $s_{i,\mathrm{y}}(t)$ are determined from s_{h}, l, and L_j.

5.3 *Joint angles in simplified model*

The joint angles in the simplified model are calculated by fitting the simplified model to the continuous curve. Let ${\phi_i}'$ and ${\psi_i}'$ be the angles of the i-th yaw joint and i-th pitch joint, respectively. The simplified model ignores some joints, which are the $2j$-th yaw joint, $2j$-th pitch joint, and $2j + 1$-th yaw joint at the j-th module, which is in anti-slip mode. In the fitting method of [22], the joint angles of an articulated mobile robot are approximately calculated by using $\kappa_{\mathrm{p}}(s)$ and $\kappa_{\mathrm{y}}(s)$ of a continuous curve. However, the method of [22] must be modified to apply it to the simplified model. If the mode of the module changes, the integration interval of the curvature of the curve of the simplified model at the calculated joint angles changes because the number of joints and the module length in the simplified model change. Therefore, we consider the four cases shown in Figure 8. The joint angle of the simplified model for each case is obtained as

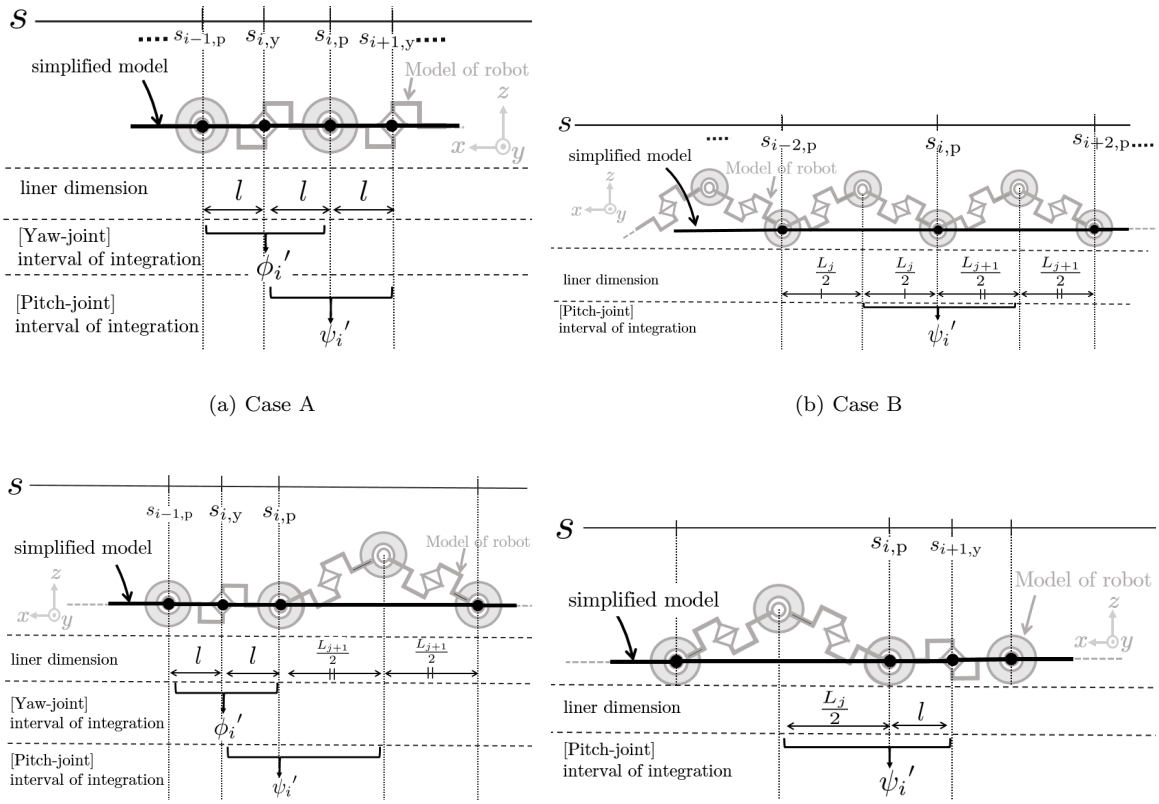

Figure 8. Integration interval of joint angle in simplified model.

follows:

$$\text{(Case A)} \quad \begin{cases} {\phi_i}' = -\displaystyle\int_{s_{i,\mathrm{y}}-l}^{s_{i,\mathrm{y}}+l} \kappa_{\mathrm{y}}(s)\mathrm{d}s \\ {\psi_i}' = -\displaystyle\int_{s_{i,\mathrm{p}}-l}^{s_{i,\mathrm{p}}+l} \kappa_{\mathrm{p}}(s)\mathrm{d}s \end{cases} \tag{3a}$$

$$\text{(Case B)} \quad {\psi_i}' = -\int_{s_{i,\mathrm{p}}-\frac{L_{j+1}}{2}}^{s_{i,\mathrm{p}}+\frac{L_j}{2}} \kappa_{\mathrm{p}}(s)\mathrm{d}s \tag{3b}$$

$$\text{(Case C)} \quad \begin{cases} {\phi_i}' = -\displaystyle\int_{s_{i,\mathrm{y}}-l}^{s_{i,\mathrm{y}}+l} \kappa_{\mathrm{y}}(s)\mathrm{d}s \\ {\psi_i}' = -\displaystyle\int_{s_{i,\mathrm{p}}-\frac{L_{j+1}}{2}}^{s_{i,\mathrm{p}}+l} \kappa_{\mathrm{p}}(s)\mathrm{d}s \end{cases} \tag{3c}$$

$$\text{(Case D)} \quad {\psi_i}' = -\int_{s_{i,\mathrm{p}}-l}^{s_{i,\mathrm{p}}+\frac{L_j}{2}} \kappa_{\mathrm{p}}(s)\mathrm{d}s \tag{3d}$$

.

Note that ${\phi_{2j}}'$, ${\psi_{2j}}'$, and ${\phi_{2j+1}}'$ of the jth anti-slip mode module are not determined in (3a)–(3d). These joints are ignored in the simplified model, as shown in Figures 8(b) and 8(d).

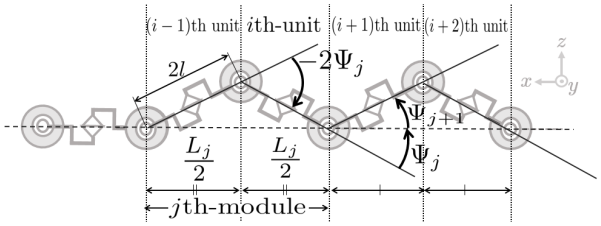

Figure 9. Joint angle for preventing robot slip in vertical pipe.

5.4 *Joint angle of realistic model*

By using $\phi_i{}'$ and $\psi_i{}'$, the joint angles of the realistic model $\phi_{i,\mathrm{d}}$, and $\psi_{i,\mathrm{d}}$ are obtained as

$$\text{(Case A)} \quad \begin{cases} \phi_{i,\mathrm{d}} = \phi_i{}' \\ \psi_{i,\mathrm{d}} = \psi_i{}' \end{cases} \tag{4a}$$

$$\text{(Case B)} \quad \psi_{i,\mathrm{d}} = \psi_i{}' + \Psi_j + \Psi_{j+1} \tag{4b}$$

$$\text{(Case C)} \quad \begin{cases} \phi_{i,\mathrm{d}} = \phi_i{}' \\ \psi_{i,\mathrm{d}} = \psi_i{}' + \Psi_{j+1} \end{cases} \tag{4c}$$

$$\text{(Case D)} \quad \psi_{i,\mathrm{d}} = \psi_i{}' + \Psi_j \tag{4d}$$

, where Ψ_j is the joint angle of the module that is in anti-slip mode, as shown in Figure 9, and is calculated as

$$\Psi_j = \cos^{-1}\left(\frac{L_j}{4l}\right). \tag{5}$$

In addition, ϕ_{2j}, ψ_{2j}, and ϕ_{2j+1} of the jth anti-slip mode module, corresponding to $\phi_{2j}{}'$, $\psi_{2j}{}'$, and $\phi_{2j+1}{}'$ in the simplified model, are calculated as

$$\begin{cases} \phi_{2j,\mathrm{d}} = 0 \\ \psi_{2j,\mathrm{d}} = -2\Psi_j \\ \phi_{2j+1,\mathrm{d}} = 0. \end{cases} \tag{6}$$

5.5 *Wheel angular velocity*

The wheel velocity depends on the wheel's location with respect to the entire robot. The angular velocity of each wheel is determined by using $s_{i,\mathrm{p}}$ at the same wheel position of the simplified model. Let $\omega_{i,\mathrm{d}}$ be the target angular velocity of the active wheel that is mounted coaxially to the i-th pitch joint. Then, $\omega_{i,\mathrm{d}}$ is designed as

$$\omega_{i,\mathrm{d}} = \frac{\dot{s}_{i,\mathrm{p}}}{r} + \dot{\Psi}_j + \omega_{\mathrm{add}}, \tag{7}$$

where r is the radius of the wheel and ω_{add} is the additional angular velocity that is used for forward and backward movement to maintain the robot's shape. The value of ω_{add} is provided by the operator to cover the positional error of the robot caused by the wheel slip. Note that $\dot{\Psi}_j$ is not zero only during extension and contraction.

If the jth module is in anti-slip mode, $\omega_{2j,\mathrm{d}}$ cannot be obtained by (7) because $s_{2j,\mathrm{p}}$ is ignored

Table 1. Parameters for forces acting on the robot's active joints and wheels.

Parameter	Notation
Static friction force	f_i
torque of joint	$\tau_{i,\mathrm{joint}}$
torque of wheel	$\tau_{i,\mathrm{wheel}}$
mass	M_m
acceleration of gravity	g
length of link	l
normal force	N_i
pitch angle	θ

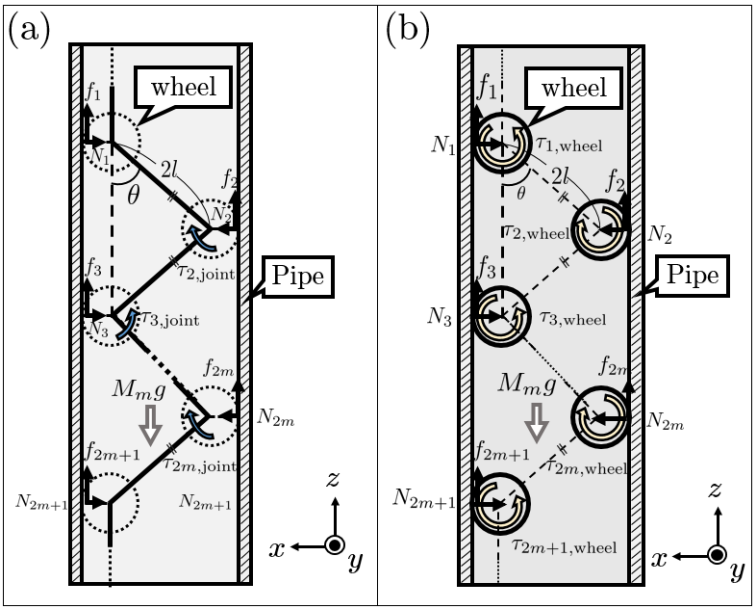

Figure 10. Forces acting on the robot's active joints and wheels. (a) Forces acting on the active joints, (b) Forces acting on the active wheels.

in the simplified model. Thus, $\omega_{2j,\mathrm{d}}$ is designed as

$$\omega_{2j,\mathrm{d}} = -\left\{ \frac{\dot{s}_{2j+1,\mathrm{p}}}{r} + \omega_{\mathrm{add}} \right\}. \tag{8}$$

The rotational direction of the wheel depends on the position at which the wheel contacts the pipe wall; for example, the rotational direction of the wheel of the first wheel axle is different from that of the wheel of the second wheel axle in Figure 5. Therefore, a minus sign is used in (8).

6. Static force analysis

We analyzed the force exerted by the modules that are in anti-slip mode. In this analysis, the mechanical component of the robot is the same as the robot used in the experiments. A conditional equation was developed for the robot to move inside a vertical pipe. We consider the case where $1, \cdots, m$-th modules are in anti-slip mode. First, the equation was developed for the case where the robot avoids slipping by using the force generated by the robot's joints. Table 1 shows the parameters and notations, and Figure 10 shows the forces and torques that act at the robot's modules.

From the equilibrium of force, the normal force when $m = 1$ and $m \geq 2$ is represented as

follows:

$$(\text{if} \quad m = 1) \quad N_i = \begin{cases} -\frac{\tau_{i+1,\text{joint}}}{4l\cos\theta} & (i = 1) \\ \frac{\tau_{i,\text{joint}}}{2l\cos\theta} & (i = 2) \\ -\frac{\tau_{i-1,\text{joint}}}{4l\cos\theta} & (i = 3) \end{cases} \tag{9}$$

$$(\text{if} \quad m \geq 2) \quad N_i = \begin{cases} -\frac{\tau_{i+1,\text{joint}}}{4l\cos\theta} & (i = 1) \\ \frac{2\tau_{i,\text{joint}}+\tau_{i+1,\text{joint}}}{4l\cos\theta} & (i = 2) \\ (-1)^i \left(\frac{\tau_{i-1,\text{joint}}+2\tau_{i,\text{joint}}+\tau_{i+1,\text{joint}}}{4l\cos\theta} \right) & (i = 3, \cdots, 2m-1) \\ \frac{\tau_{i-1,\text{joint}}+2\tau_{i,\text{joint}}}{4l\cos\theta} & (i = 2m) \\ -\frac{\tau_{i-1,\text{joint}}}{4l\cos\theta} & (i = 2m+1). \end{cases} \tag{10}$$

The total mass of the robot as M_m is obtained as

$$M_m = (2m+1)M_{\text{unit}} + M_{\text{cable}}, \tag{11}$$

where M_{unit} and M_{cable} are the mass of one unit and the cable, respectively.

In each unit of the actual robot used in the experiments, the active wheel is attached to the robot on one side and the passive wheel is attached to the robot on the other side. All the active wheels are not on the same side of the robot, they alternate. The passive wheel cannot prevent the robot from slipping. Therefore, the maximum static frictional force of i-th unit is represented as

$$f_i = \frac{1}{2}\mu|N_i|, \tag{12}$$

where μ is the coefficient of the maximum static frictional force. If all modules are in anti-slip mode, the condition where the robot avoids slipping is obtained as follows from (10) and (12):

$$\sum_{i=1}^{2m+1} f_i = \frac{\mu}{2} \frac{\sum_{i=2}^{2m} \tau_{i,\text{joint}}}{l\cos\theta} \geqq M_m g. \tag{13}$$

As the robot moves inside a vertical pipe, each active wheel has to satisfy the following condition:

$$F_{m,\text{wheel}} = \frac{\sum_{i=1}^{2m+1} \tau_{i,\text{wheel}}}{r} \geqq M_m g. \tag{14}$$

The robot can move inside vertical pipe without slipping by satisfying (13) and (14). Dynamic force analysis and dynamics-based design are left as topics for future study.

7. Experiments

Experiments were carried out to demonstrate the effectiveness of the control method. We used a robot that was an improved version of the robot in [26]. Figure 11 shows the robot, and Table 2 provides the robot's parameters. The configuration of the joints and wheels of the robot are the same as that in the model. Each active wheel is driven by a servomotor through a timing belt attached to one side of each unit. Dynamixel MX-64 servomotors were used for active joints and wheels [31]. The computer sent control input to the servomotors and received the angles of servomotor postures by RS485 serial communications. Electrical power was supplied by the

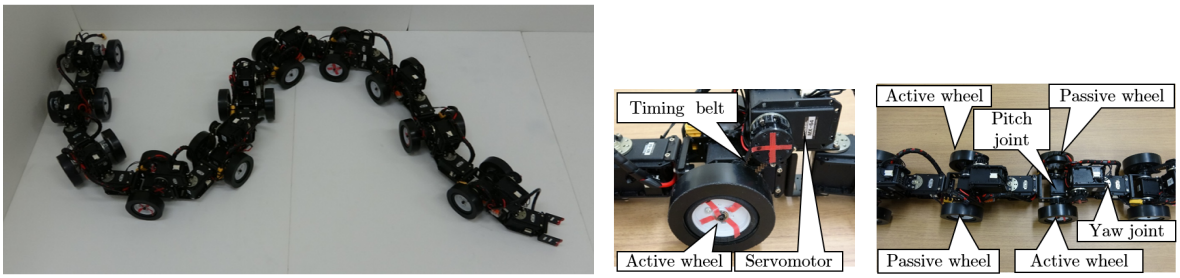

(a) Overview. (b) Active wheel. (c) Joints and wheels.

Figure 11. Robot used for experimental verification.

Table 2. Parameters of the robot

Parameter	Value
Number of module m	5
Number of unit n	11
Number of yaw joints	11
Number of pitch joints	10
Length of link l[mm]	88
Wheel radius [mm]	37.5
Total mass[a] [kg]	8.99
Torque of servomotor[b] [N · m]	7.30

[a]The total mass includes the body of the robot and cables.

[b]Torque of servomotor is stall-torque at 14.8V, 5.2A [31].

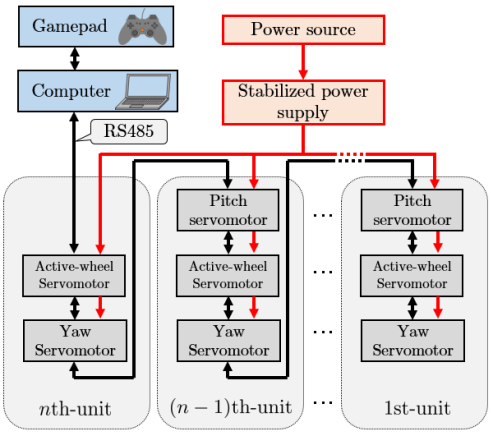

Figure 12. Robot data communication systems and power supply wiring.

wiring system. The operator provided the robot with the input commands using a gamepad. Figure 12 shows an overview of the communications system and electrical power supply. Figures 13 shows the piping, consisting of a curved pipe (VUDL200) or branched pipe (VUDT200), and two straight pipes.

7.1 *Number of modules*

When the robot moves in a curved pipe, not all the modules are in anti-slip mode because some modules are in normal mode. Let m be the total number of modules and m' be the number of modules in anti-slip mode. When the robot moves through the VUDL200 or VUDT200 pipe, three modules have to be in normal mode. We consider the case where the $1, \cdots, m'$-th modules

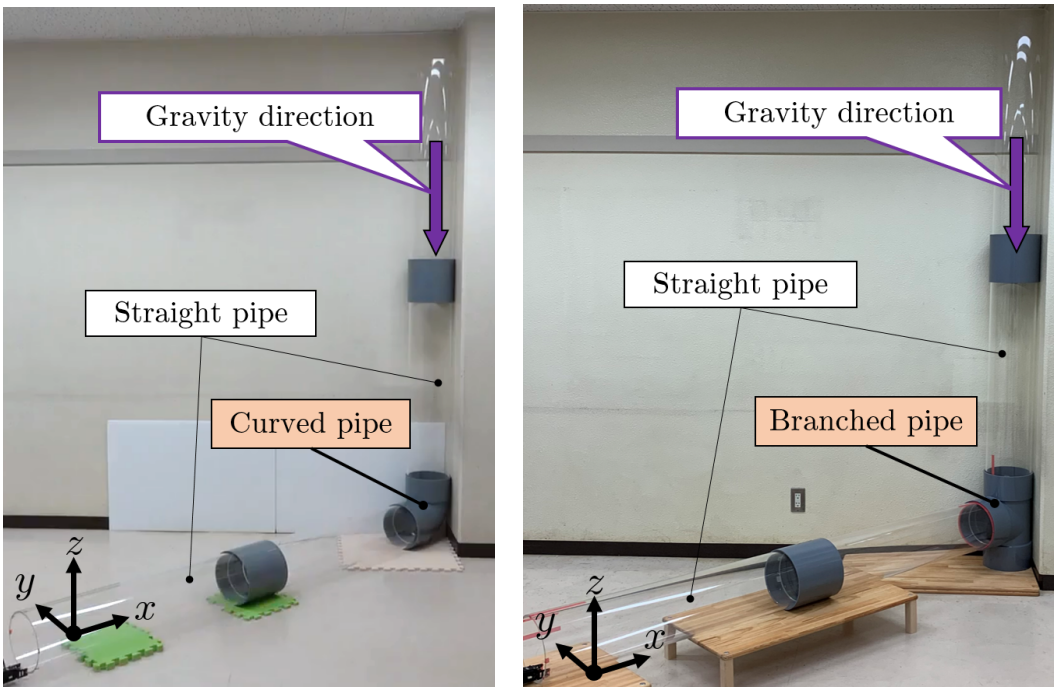

(a) Piping consisting of a curved pipe (VUDL200) and two straight pipes.

(b) Piping consisting of a branched pipe (VUDT200) and two straight pipes.

Figure 13. Experimental environment.

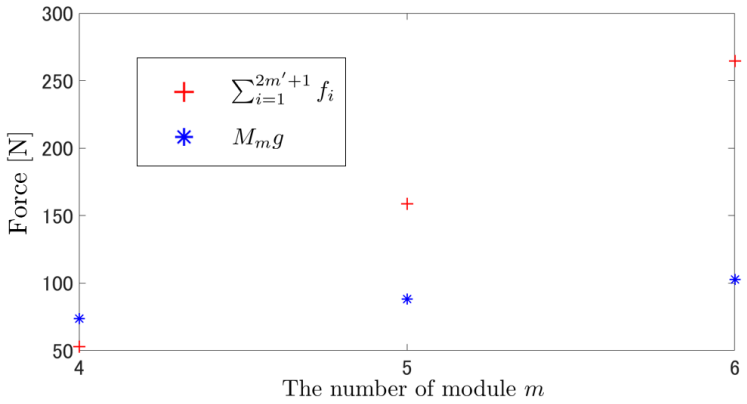

Figure 14. Results for $\sum_{i=1}^{2m'+1} f_i$ and $M_m g$

in order from the head are in anti-slip mode and the other modules are in normal mode. We assume that the friction force generated by the modules in normal mode is zero.

We obtained $\sum_{i=1}^{2m+1} f_i$ in (13) by experimental measurement. In this experiment, we used a robot consisting of only one module in a vertical straight pipe. We measured the static frictional force while pulling on the robot with a rope when the module was in anti-slip mode. Then, we calculated $\sum_{i=1}^{2m'+1} f_i$ and $M_m g$ at $(m, m') = (4, 1), (5, 2), (6, 3)$, and the experimental results are shown in Figure 14.

Next, we calculated $F_{m,\text{wheel}}$ in (14) from Table 2. In the case of $m = 5$ and $m' = 2$, we obtained $F_{m',\text{wheel}}$=973.33[N] and $M_m g = 88.17$[N].

From these results, we found that (13) and (14) were satisfied at $m \geq 5$. Thus, we used $m = 5$

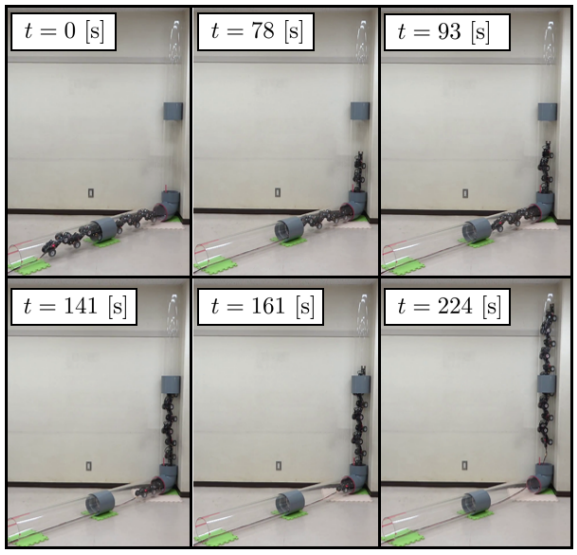

Figure 15. Experimental result for moving inside pipes in case 1.

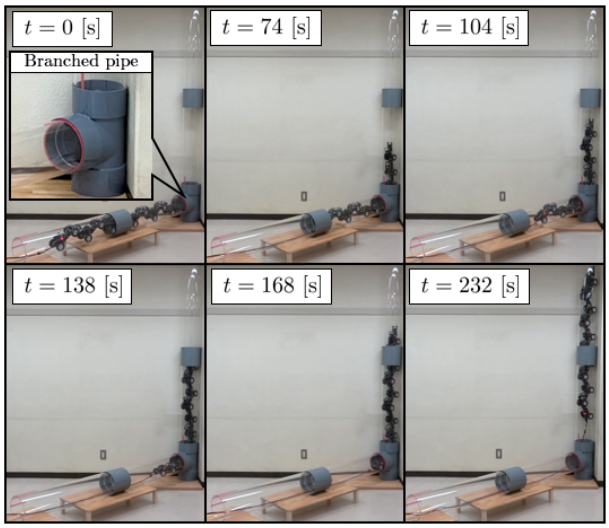

Figure 16. Experimental result for moving inside pipes in case 2.

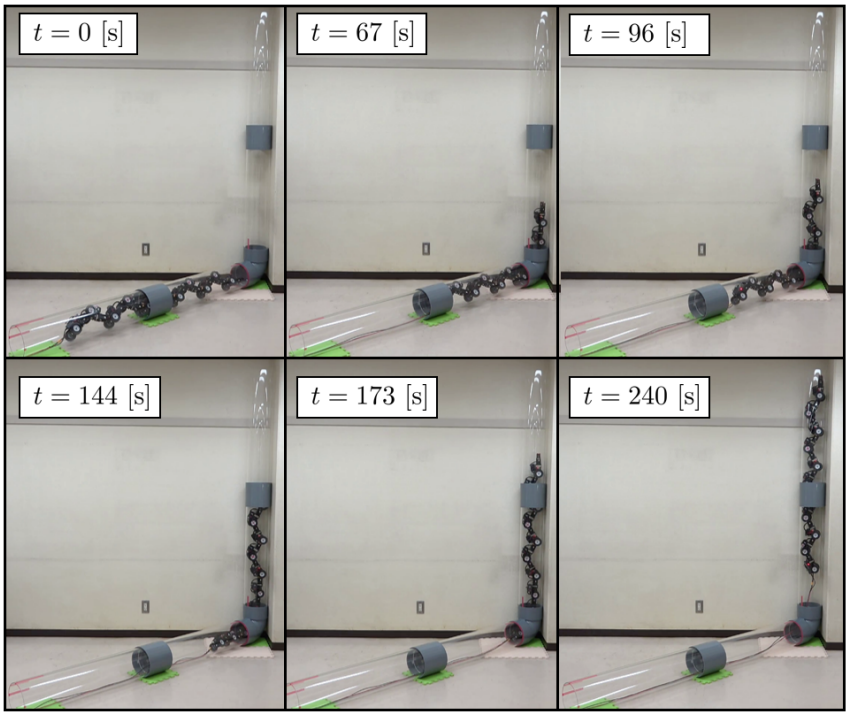

Figure 17. Experimental result for moving inside pipes in case 3.

as the number of modules for the experiments for in-pipe locomotion.

7.2 *In-pipe locomotion*

Figures 13 shows the experimental setup. In Figures 13, the x-y plane is parallel to the ground and the x-axis is parallel to a straight pipe placed on the ground. Table 2 shows the robot parameters.

We carried out experiments for six cases. In case 1 the initial posture of the robot was not rotated around the x-axis and a curved pipe (VUDL200) was used. In case 2, the initial posture

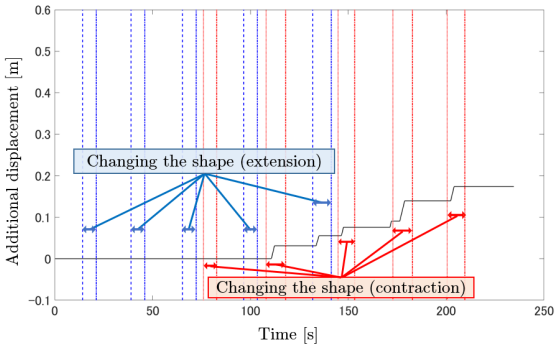

(a) Case 1

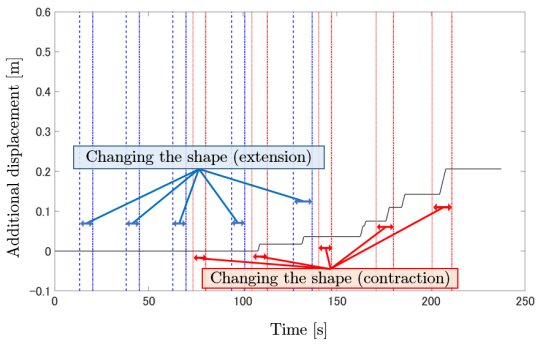

(b) Case 2

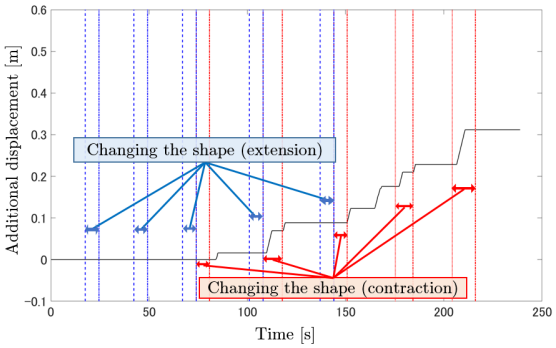

(c) Case 3

Figure 18. Additional angular velocity ω_{add} of the active wheels in cases 1–3.

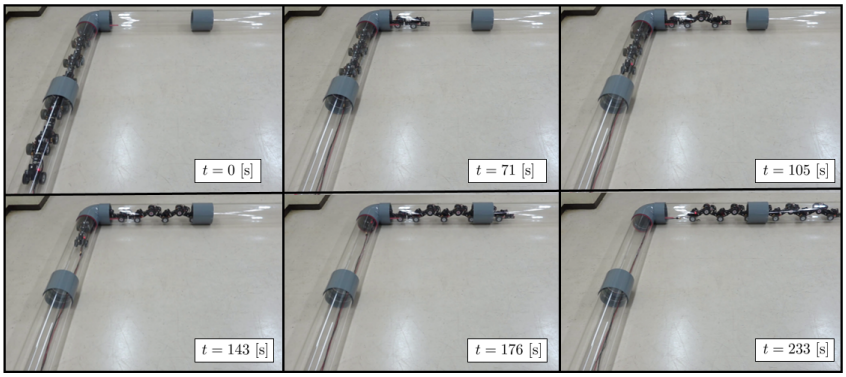

Figure 19. Experimental result for moving inside horizontal pipes in case 4.

of the robot was not rotated around the x-axis and a branched pipe (VUDT200) was used. In cases 3 and 4, the posture was rotated $-\pi/4$[rad] and $-\pi/2$[rad] around the x-axis, respectively, and a curved pipe (VUDL200) was used. In cases 1–4, the initial position of the robot was inside the straight pipe before the entrance of the curved pipe. The target continuous curve in cases 1, 2 and 4 was designed so that the robot followed the wall inside the piping. In case 3, the target continuous curve was designed to pass through the center axis of the cross-section of piping. The experiments in case 1–4 were conducted three times for each case.

Figures 15, 16 and 17 show the results for cases 1, 2 and 3, respectively. All modules were in

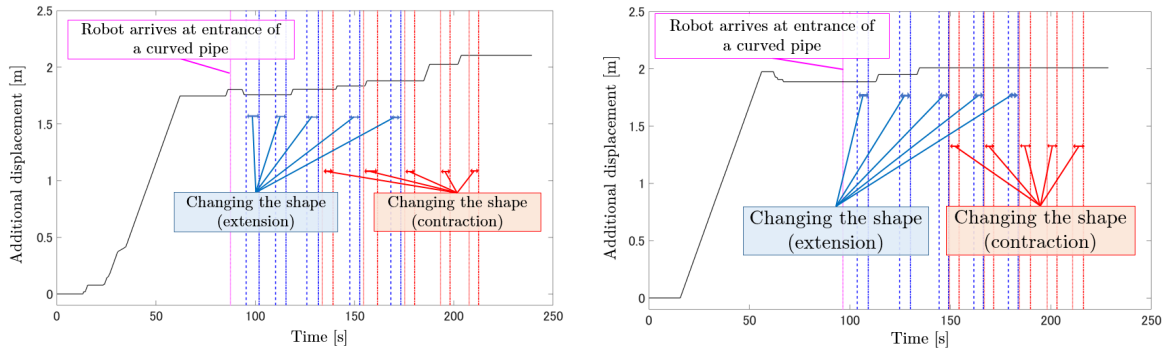

(a) Case 5 (b) Case 6

Figure 20. Additional angular velocity ω_{add} of the active wheels in cases 5 and 6.

anti-slip mode inside the straight pipe at the initial position. The mode of each module changed from anti-slip to normal when it reached the entrance of the curved pipe. Each module was in normal mode when it was inside the curved pipe. The mode of each module changed from normal to anti-slip after passing through the curved pipe. As a result, the robot could move through the straight, curved and branched pipes adopting the proposed method.

However, the operator needed to input an additional rotational velocity for the active wheels ω_{add} to make the in-pipe locomotion successful. The main reason for this problem was an error between the target position and the actual position. Figures 18(a), 18(b) and 18(c) show the time integration of ω_{add}. The input was almost always needed for the robot to be moving forward, which means that the robot could not track the target. The main reason for this was slipping of the timing belts between the active wheel and its servomotor. We heard the timing belt slipping after the robot entered the vertical straight pipe. When the belt slips, the robot cannot obtain the drive force from the servomotor through the timing belt. If the slippage could be suppressed, the error between the target position and the actual position would decrease. However, the error cannot be completely eliminated because the robot has feedforward control. If the position of the robot were estimated by the method used in [32], the additional rotational velocity inputted by the operator would not be necessary.

We carried out additional experiments in case 4, where the initial posture of the robot was rotated $-\pi/2$[rad] around the x-axis. In the experiments, we used the curved pipe (VUDL200) shown in Figure 13 (a) . The result was that the robot could not pass through the piping. A wheel of the robot became stuck in the gap between the straight and curved pipes when the first and second modules were in normal mode. As a result, the urethane rubber on the wheel came off, and the module in anti-slip mode could not appropriately make contact with the wall of the piping. In addition, there was an overload error for the actuators of the robot, and some actuators stopped their motion. The reason why the wheel became stuck at the clearance gap of the joint of the pipe is that some modules in normal mode droop under gravity. This was a result of the lack of torque of the actuator used in the robot's joint. When the first and second modules are in normal mode such that the modules can enter the curved pipe, the yaw joint in the fifth unit receives the weight of the first to fourth units. However, the modules from the first to fourth units droop under gravity because of insufficient joint torque. It is expected that the robot follows the target path if the joint torque is sufficient. In addition, we carried out experiments in a horizontal pipe as shown in Figure 19. In this case, the modules in normal mode do not droop under gravity and the robot maintains its posture. In the experiment, the robot could locomote within the piping. It was thus confirmed that the robot can locomote in piping using the proposed method if the joint torque of the robot is sufficiently large to maintain the posture of the robot under the effect of gravity. Additional experiments were carried out to demonstrate

the effectiveness of the developed interface system. Case 5 had the same experimental conditions as case 1 while case 6 had the same conditions as case 4, with the operator using the interface system in cases 5 and 6. In case 6, we carried out experiments in a horizontal pipe as shown in Figure 19. In cases 5 and 6, the robot moved to the entrance of the curved pipe using ω_{add} and moved in the pipe using $s_{\mathrm{h,add}}$ and ω_{add}. The skill level of the operator was low because it was the first time that the operator had operated the robot. The operator operated the robot only looking at the view provided by the camera and the interface system. The robot succeeded in passing through in the piping in cases 5 and 6. Figure 20(a) and (b) shows the time integration of ω_{add}. In this experiment, ω_{add} was also used to move to the initial position. Therefore, as shown in Figure 20(a) and (b), the input before the robot arrived at the entrance of the curved pipe was the input used to adjust the initial position. The operator adjusted the head position of the robot to the entrance of the curved pipe according to the view of the camera. In addition, the operator understood the difference between the present posture and target posture (i.e., error) using the interface system and corrected the position of the robot using ω_{add}.

8. Conclusions

This paper proposed a control method in which an articulated wheeled mobile robot moves inside a pipe. The robot used two different shapes, anti-slip and normal, for each module. Modules in anti-slip mode prevent the robot from slipping inside a straight vertical pipe. Modules in normal mode allow movement through a curved pipe. The robot can move between straight and curved pipes by switching modules between the two modes. The module mode switching was based on a simplified model. The effectiveness of the control method was demonstrated by experiments. The practical use of the robot in an actual pipe requires us to develop a method in which the operator does not need to adjust the input velocity and to improve the robot for various types of actual piping. These tasks are left as future work. An operator used an interface system that we developed to pass a robot through piping without directly looking at the robot or see-through pipe. The target continuous curve corresponding to the curved pipe comprised pre-designed curves. It is considered that the robot can move in a pipeline using the proposed method if the operator selects a target curve from various pre-designed curves as to fit a curved pipe or branched pipe.

Acknowledgments

This work was partially supported by the ImPACT Program of the Council for Science, Technology and Innovation (Cabinet Office, Government of Japan), and the Japan Society for the Promotion of Science, Kakenhi Grant 18K04011. We thank Bryan Schmidt from Edanz Group (www.edanzediting.com/ac) for editing a draft of this manuscript.

References

[1] Mirats Tur JM, Garthwaite W. Robotic Devices for Water Main In-Pipe Inspection: A Survey. Journal of Field Robotics; 2010;27(4):491–508.
[2] Roh SG,Choi HR. Differential-drive in-pipe robot for moving inside urban gas pipelines. IEEE transactions on robotics; 2005;21(1):1–17.
[3] Kwon YS, Yi BJ. Design and motion planning of a two-module collaborative indoor pipeline inspection robot. IEEE Transactions on Robotics; 2012;28(3):681–696.
[4] Schempf H, Mutschler E, Gavaert A, Skoptsov G, Crowley W. Visual and nondestructive evaluation inspection of live gas mains using the Explorer$^{\mathrm{TM}}$ family of pipe robots. Journal of Field Robotics; 2010; 27(3):217–249.

[5] Debenest P, Guarnieri M, Hirose S. PipeTron series-Robots for pipe inspection. In: Proceedings of the 2014 3rd International Conference on Applied Robotics for the Power Industry; Foz do Iguassu, Brazil; 2014 Oct 14–16; p.1–6.
[6] Kakogawa A, Ma S. Design of a multilink-articulated wheeled pipeline inspection robot using only passive elastic joints. Advanced Robotics; 2017; 32(1):37–50.
[7] Dertien E, Stramigioli S, Pulles K. Development of an inspection robot for small diameter gas distribution mains. In: 2011 IEEE International Conference on Robotics and Automation; Shanghai, China; 2011 May 9–13;p. 5044–5049.
[8] Kuwada A, Wakimoto S, Suzumori K, Adomi Y. Automatic Pipe Negotiation Control for snake-like robot. In: 2008 IEEE/ASME International Conference on Advanced Intelligent Mechatronics; Xian, China; 2008 Jul 2–5;p. 558–563.
[9] Barazandeh F, Bahr B, Moradi A. Investigation of Self-locking In Concertina Movement. In: 2007 Mediterranean Conference on Control & Automation; Athens, Greece; 2007 June 27–29.
[10] Shin H, Jeong KM, Kwon JJ. Development of a Snake Robot Moving in a Small Diameter Pipe. In: International Conference on Control, Automation and Systems (ICCAS) 2010; Gyeonggi-do, South Korea; 2010 Oct 27–30;p. 1826–1829.
[11] Rollinson D, Choset H. Pipe Network Locomotion with a Snake Robot. Journal of Field Robotics; 2016;30(3):322–336.
[12] Kamegawa T, Baba T, Gofuku A. V-shift control for snake robot moving the inside of a pipe with helical rolling motion. In: 2011 IEEE International Symposium on Safety, Security, and Rescue Robotics; Kyoto, Japan; 2011 Nov 1–5;p. 1–6.
[13] Xiao S, Bingy Z, Huang K, Huang Y. Snake-like Robot Climbs Inside Different Pipes. In: 2017 IEEE International Conference on Robotics and Biomimetics (ROBIO); Macau, China; 2017 Dec 5–8;p. 1–8.
[14] Takemori T, Tanaka M, Matsuno F. Gait Design for a Snake Robot by Connecting Curve Segments and Experimental Demonstration. IEEE Transactions on Robotics; 2018;34(5);1384–1391.
[15] Gray J. The Mechanism of Locomotion in Snakes. Journal of Experimental Biology; 1946;23(2):101–120.
[16] Qi W, Kamegawa T, Gofuku A. Proposal of helical wave propagate motion for a snake robot to across a branch on a pipe. In: 2016 IEEE/SICE International Symposium on System Integration (SII); Sapporo, Japan; 2016 Dec 13–15;p. 821–826.
[17] Takemori T, Tanaka M, Matsuno F. Ladder Climbing with a Snake Robot. In: 2018 IEEE/RSJ International Conference on Intelligent Robots and Systems (IROS); Madrid, Spain; 2018 Oct 1–5;p. 8140–8145.
[18] Fjerdingen SA, Liljebäck P, Transeth AA. A snake-like robot for internal inspection of complex pipe structures (PIKo). In: 2009 IEEE/RSJ International Conference on Intelligent Robots and Systems; St. Louis, MO, USA; 2009 Oct 10–15;p. 5665–5671.
[19] Borenstein J, Hansen M, Borrell A. The OmniTread OT-4 Serpentine Robot: Design and Performance. Journal of Field Robotics; 2017;24(7):601–621.
[20] Tanaka M, Nakajima M, Suzuki Y, Tanaka K. Development and Control of Articulated Mobile Robot for Climbing Steep Stairs. IEEE/ASME Transactions on Mechatronics; 2018;23(2):531–541.
[21] Tanaka M, Tadakuma K, Nakajima M, Fujita M. Task-space Control of Articulated Mobile Robots with a Soft Gripper for Operations. IEEE Transactions on Robotics; 2019;35(1):135–146.
[22] Yamada H, Hirose S. Study of Active Cord Mechanism -Approximations to Continuous Curves of a Multi-joint Body-. Journal of the Robotics Society of Japan; 2008;26(1):110–120. (in Japanese with English summary).
[23] Chirikjian GS, Burdick JW. A Modal Approach to Hyper-Redundant Manipulator Kinematics. IEEE Transaction on Robotics and Automation; 1994;10(3):343–354.
[24] Kano T, Yoshizawa R, Ishiguro A. *Tegotae*-based decentralised control scheme for autonomous gait transition of snake-like robots. Bioinspiration & biomimetics; 2017;12(4):046009.
[25] Kano T, Yoshizawa R, Ishiguro A. Snake-Like Robot that Can Generate Versatile Gait Patterns by Using *Tegotae*-Based Control. In: Vouloutsi V. et al. (eds) Biomimetic and Biohybrid Systems. Living Machines 2018. Lecture Notes in Computer Science, vol 10928. Springer, Cham; 2018;p. 249–254.
[26] Tanaka M, Nakajima M, Tanaka K. Smooth control of an articulated mobile robot with switching constraints. Advanced Robotics; 2016;30(1):29–40.
[27] Yamada H, Takaoka S, Hirose S. A snake-like robot for real-world inspection applications (the design and control of a practical active cord mechanism). Advanced Robotics; 2013;27(1):47–60.

[28] Kouno K, Yamada H, Hirose S. Development of Active-Joint Active-Wheel High Traversability Snake-Like Robot ACM-R4.2. Journal of Robotics and Mechatronics; 2013;25(3):559–566.
[29] Yamada H, Hirose S. Study on the 3D Shape of Active Cord Mechanism. In: Proceedings 2006 IEEE International Conference on Robotics and Automation, 2006. ICRA 2006; Orlando, FL, USA; 2006 May 15–19;p. 2890–2895.
[30] COPPELIA ROBOTICS. V-REP. [cited 2019 May 2]. Available from:http://www.coppeliarobotics.com/index.html.
[31] ROBOTIS. MX-64 - ROBOTIS e-MANUAL. 2010 [cited 2018 Nov 4]. Available from: http://support.robotis.com/jp/product/dynamixel/mx_series/mx-64.html.
[32] Bando Y, Suhara H, Tanaka M, Kamegawa T, Itoyama K, Yoshii K, Matsuno F, Okuno HG. Sound-based Online Localization for an In-pipe Snake Robot. In: 2016 IEEE International Symposium on Safety, Security, and Rescue Robotics (SSRR); Lausanne, Switzerland; 2016 Oct. 23-27;p. 207–213.